On Outage Probability for Two-User Fluid Antenna Multiple Access

Hao Xu, Kai-Kit Wong, Wee Kiat New, and Kin-Fai Tong
Department of Electronic and Electrical Engineering, University College London, London, United Kingdom
E-mail: {hao.xu, kai-kit.wong, a.new, k.tong}@ucl.ac.uk

***Abstract*—Fluid antenna system (FAS) is an emerging flexible antenna technology that provides a new way for multiple access. In fluid antenna multiple access (FAMA), each user switches its fluid antenna to the location (i.e., port) in which the interfering users suffer from a deep fade for interference-free communication. Previous work has attempted to understand the interference immunity of FAMA but the results are limited to simplified spatial correlation models. In this paper, we revisit the FAMA system with only two users by characterizing the joint spatial correlation amongst all the ports. Using this model, however, the number of variables determining each channel coefficient scales with that of ports, hence making the analysis intractable. To tackle this, we first show that the channel model could be considerably simplified by taking into account only a few variables, and then derive the outage probability for the considered FAMA system by using the approximated model. Simulation results show that the simplified channel model can quickly approach the exact one and that the outage probability decreases with the number of ports but has an error floor unless the size of fluid antenna is increased.**

***Index Terms*—FAMA, Fluid antenna, Slow fluid antenna multiple access, Outage probability, Spatial correlation.**

I. Introduction

The advances in mobile communications have seen many multiple access technologies get developed, with both massive multiple-input multiple-output (MIMO) antenna [1] and non-orthogonal multiple access (NOMA) [2] being the latest additions that many believe could address the massive connectivity challenge in 5G and beyond systems [3]. The fact that the base station (BS) needs to acquire the channel state information (CSI) and perform complex precoding optimization, however, greatly affects the scalability of massive MIMO. Similarly, for NOMA, the CSI is also required at the BS for power control as well as user clustering and worse, multiuser detection such as successive interference cancellation (SIC) is needed at each NOMA user to deal with the interference for high capacity.

To overcome these challenges, a new multiple access technique, referred to as fluid antenna multiple access (FAMA), is recently proposed [4], [5]. This is motivated by the recent advances in flexible antenna technologies, e.g., [6]–[10] that offer unprecedented reconfigurability. Under the name 'fluid antenna', recent studies in [11]–[16] investigated a single-user system in which the receiving fluid antenna can switch its location to the best of N fixed ports within a given space. In so doing, the receiver can avoid channel deep fades. Multiple access using fluid antenna was first proposed in [17]. It takes advantage of the fact that multiuser signals fade independently in space and the fluid antenna at a user terminal can find a port (or location) in which the interfering users all fade to have an interference-free channel for communication. It was reported that fast FAMA could support hundreds of users on the same time-frequency channel [17], [18] while slow FAMA could handle a few users [19]. The difference between fast and slow FAMA is that in fast FAMA, the fluid antenna switches to the best port on a symbol-by-symbol basis whereas the slow version updates its best port only when the channel changes.

Despite the recent interest, the analytical results available so far appear to be based on a simplified channel model [18], [20] which does not accurately characterize the spatial correlation amongst the ports of the fluid antenna, and could result in an overly optimistic performance estimate. Most recently in [21], Khammassi *et al.* presented the outage performance analysis for a single-user fluid antenna system (FAS) by using a fully correlated channel model that could account for the correlation of the channels between any two ports accurately. Their results indicate that the performance of FAS is limited by the size of the fluid antenna and increasing N has a diminishing return.

In this paper, we revisit the two-user FAMA system[1] and our aim is to analyze the outage probability performance when the fully correlated channel model in [21] is used. As we will show later, the channel model and correlation among different ports are determined by a Hermitian Toeplitz matrix $\boldsymbol{\Sigma}$, whose elements can be obtained according to the Jake's model [22]. We further illustrate that the energy of $\boldsymbol{\Sigma}$ is mainly focused on a few largest eigenvalues. It is thus possible to approximate each channel coefficient by taking only a few eigenvalues into account. As such, it allows us to derive the outage probability using the approximated model. Simulation results validate the approximation and indicate that the outage probability of two-user FAMA exhibits similar characteristics in terms of the number of ports, N, and size of the fluid antenna.

II. System Model and Problem Formulation

Consider a downlink FAS system with a BS and two users. The BS has two fixed antennas, where each of them serves a user, and each user is equipped with a fluid antenna. The location of the fluid antenna can be switched instantly to one of the N preset ports, which are evenly distributed along a linear dimension of length $W\lambda$ and share a common RF chain. Here W denotes the normalized size of the fluid antenna and λ

[1]For the two-user case where noise is ignored (which we assume in this paper), fast FAMA and slow FAMA are the same. For differences of fast and slow FAMA, readers are referred to [4].

is the wavelength. Without loss of generality, we assume that the k-th antenna at the BS serves user k. Then the received signal at the n-th port of user k is given by

$$y_k^{(n)} = \sum_{j=1}^{2} g_{j,k}^{(n)} s_j + \eta_k^{(n)}, \text{ for } k = 1, 2, \tag{1}$$

where $g_{j,k}^{(n)} \sim \mathcal{CN}(0, \sigma_{j,k}^2)$ is the channel gain from the j-th BS antenna to the n-th port of user k, $s_j \sim \mathcal{CN}(0, p_j)$ denotes the data symbol intended for user j, and $\eta_k^{(n)} \sim \mathcal{CN}(0, \sigma_0^2)$ denotes the additive white Gaussian noise.

Denoting the channel vector $\boldsymbol{g}_{j,k} = (g_{j,k}^{(1)}, \ldots, g_{j,k}^{(N)})^T$ and its covariance matrix by $\boldsymbol{\Sigma}_{j,k} = \sigma_{j,k}^2 \boldsymbol{\Sigma}$, we characterize the spatial correlation of the ports by following the Jake's model [22] so that the (n, n')-th element of $\boldsymbol{\Sigma}$ is given by

$$(\boldsymbol{\Sigma})_{n,n'} = \frac{1}{\sigma_{j,k}^2} \text{Cov}\left[g_{j,k}^{(n)}, g_{j,k}^{(n')}\right] = J_0\left(2\pi(n-n')\Delta\right), \tag{2}$$

where $\Delta = W/(N-1)$ is the normalized distance between any two adjacent ports and $J_0(\cdot)$ is the zero-order Bessel function of the first kind. To analyze the system performance, we need to model the channel coefficients such that they satisfy the distribution and the correlation characteristics given above.

Denote the eigen-decomposition of $\boldsymbol{\Sigma}$ by $\boldsymbol{U}\boldsymbol{\Theta}\boldsymbol{U}^H$, where $\boldsymbol{U}$ is a unitary matrix and $\boldsymbol{\Theta} = \text{diag}\{\theta_1, \ldots, \theta_N\}$ denotes the eigenvalue matrix. Assume that the eigenvalues in $\boldsymbol{\Theta}$ are arranged in descending order, i.e., $\theta_1 \geq \cdots \geq \theta_N$. Let

$$\boldsymbol{g}_{j,k} = \sigma_{j,k} \boldsymbol{U} \boldsymbol{\Theta}^{\frac{1}{2}} \boldsymbol{x}_{j,k}, \tag{3}$$

where $\boldsymbol{x}_{j,k} = (x_{j,k}^{(1)}, \ldots, x_{j,k}^{(N)})^T$ and $x_{j,k}^{(n)} \sim \mathcal{CN}(0, 1)$. Note that $x_{j,k}^{(n)}$ can also be expressed as $x_{j,k}^{(n)} = a_{j,k}^{(n)} + i b_{j,k}^{(n)}$, where $a_{j,k}^{(n)}$ and $b_{j,k}^{(n)}$ are independent and identically distributed (i.i.d.) real Gaussian variables with zero-mean and variance $\frac{1}{2}$. The n-th element of $\boldsymbol{g}_{j,k}$, i.e., $g_{j,k}^{(n)}$, can thus be expressed as

$$\begin{aligned} g_{j,k}^{(n)} &= \sigma_{j,k} \sum_{m=1}^{N} \sqrt{\theta_m} u_{n,m} x_{j,k}^{(m)} \\ &= \sigma_{j,k} \sum_{m=1}^{N} \sqrt{\theta_m} u_{n,m} \left(a_{j,k}^{(m)} + i b_{j,k}^{(m)}\right). \end{aligned} \tag{4}$$

When $n' = n$ in (2), $(\boldsymbol{\Sigma})_{n,n} = 1$. Hence, $\sum_{m=1}^{N} \theta_m u_{n,m}^2 = (\boldsymbol{\Sigma})_{n,n} = 1$. It is therefore known from (3) and (4) that $g_{j,k}^{(n)} \sim \mathcal{CN}(0, \sigma_{j,k}^2)$ and $\mathbb{E}\left[\boldsymbol{g}_{j,k} \boldsymbol{g}_{j,k}^H\right] = \sigma_{j,k}^2 \boldsymbol{\Sigma}$. Therefore, the models in (3) and (4) can perfectly characterize the distribution of the channel gains and the spatial correlation of the ports.

For user k, its signal-to-interference plus noise ratio (SINR) at the n-th port is found as

$$\gamma_k^{(n)} = \frac{p_k |g_{k,k}^{(n)}|^2}{p_{\bar{k}} |g_{\bar{k},k}^{(n)}|^2 + \sigma_0^2} \overset{(a)}{\approx} \frac{p_k |g_{k,k}^{(n)}|^2}{p_{\bar{k}} |g_{\bar{k},k}^{(n)}|^2}, \tag{5}$$

where $\bar{k} = 1$ if $k = 2$ and $\bar{k} = 2$ if $k = 1$, and (a) assumes that the interference power is much greater than the noise power. Though SINR is a more accurate performance measure, signal-to-interference ratio (SIR) is a good approximation for interference-limited environments. Our objective is to obtain the outage probability of the FAMA system, given by

$$\begin{aligned} p_{\text{out},k}(r_k) &= \Pr\left\{ \max\left\{ \frac{|g_{k,k}^{(1)}|^2}{|g_{\bar{k},k}^{(1)}|^2}, \ldots, \frac{|g_{k,k}^{(N)}|^2}{|g_{\bar{k},k}^{(N)}|^2} \right\} < \frac{\gamma_{\text{th}} p_{\bar{k}}}{p_k} \right\} \\ &= \Pr\left\{ \frac{|g_{k,k}^{(1)}|}{|g_{\bar{k},k}^{(1)}|} < r_k, \ldots, \frac{|g_{k,k}^{(N)}|}{|g_{\bar{k},k}^{(N)}|} < r_k \right\}, \end{aligned} \tag{6}$$

where γ_{th} denotes the SIR threshold and $r_k \triangleq \sqrt{\gamma_{\text{th}} p_{\bar{k}} / p_k}$.

III. Main Results

In this section, we analyze the outage probability of the two-user FAMA system. Although (3) or (4) can characterize perfectly the distribution of the channel gains and the spatial correlation among the ports, each element $g_{j,k}^{(n)}$ in $\boldsymbol{g}_{j,k}$ consists of $2N$ independent Gaussian variables, i.e., $a_{j,k}^{(m)}$ and $b_{j,k}^{(m)}$, making further analysis intractable since N is usually very large. Hence, in the following, we first simplify or approximate $g_{j,k}^{(n)}$ and then analyze the outage probability.

A. Approximation of the Channel Model

It can be found that the channel model (4) is mainly determined by $\boldsymbol{\Sigma}$, which on one hand, ensures $g_{j,k}^{(n)} \sim \mathcal{CN}(0, \sigma_{j,k}^2)$ since $(\boldsymbol{\Sigma})_{n,n} = \sum_{m=1}^{N} \theta_m u_{n,m}^2 = 1$, and on the other hand, determines the correlation of the elements in $\boldsymbol{g}_{j,k}$. Also, from (2), we see that $\boldsymbol{\Sigma}$ is a Hermitian Toeplitz matrix. Since N is large here, as we will show later, $\theta_1 \gg \theta_N$ and only a few eigenvalues are significant, making it possible to approximate $g_{j,k}^{(n)}$ by taking only a few eigenvalues into account. Specifically, we consider the largest $L \ll N$ eigenvalues in (4) and neglect the other terms so that we have

$$\tilde{g}_{j,k}^{(n)} = \sigma_{j,k} \sum_{m=1}^{L} \sqrt{\theta_m} u_{n,m} \left(a_{j,k}^{(m)} + i b_{j,k}^{(m)}\right). \tag{7}$$

Then, an important question is to what extent $\tilde{g}_{j,k}^{(n)}$ can approximate $g_{j,k}^{(n)}$. To answer this question, we define a threshold θ_{th} for the eigenvalues of $\boldsymbol{\Sigma}$ and step function

$$H(\theta, \theta_{\text{th}}) \triangleq \begin{cases} 1, & \theta > \theta_{\text{th}}, \\ 0, & \theta \leq \theta_{\text{th}}. \end{cases} \tag{8}$$

In addition, we define

$$\begin{cases} D_N(\theta_{\text{th}}) \triangleq \dfrac{1}{N} \displaystyle\sum_{n=1}^{N} H(\theta_n, \theta_{\text{th}}), \\ S_N(\theta_{\text{th}}) \triangleq \dfrac{1}{N} \displaystyle\sum_{n=1}^{N} \theta_n H(\theta_n, \theta_{\text{th}}). \end{cases} \tag{9}$$

Obviously, $D_N(\theta_{\text{th}})$ can be seen as the proportion of eigenvalues greater than θ_{th} and $S_N(\theta_{\text{th}})$ is the average value of them. We give their limits in the following theorem.

Theorem 1. *As the number of ports N grows large, the limits of $D_N(\theta_{th})$ and $S_N(\theta_{th})$ are, respectively, approximated as*

$$\lim_{N\to+\infty} D_N(\theta_{th}) \approx \frac{1}{2\pi}\int_{-\pi}^{\pi} \hat{H}(f(x),\theta_{th})dx, \tag{10}$$

$$\lim_{N\to+\infty} S_N(\theta_{th}) \approx \frac{1}{2\pi}\int_{-\pi}^{\pi} f(x)\hat{H}(f(x),\theta_{th})dx, \tag{11}$$

where $f(x)$, given in (20), is an exponential-form Fourier series, and $\hat{H}(\theta,\theta_{th})$, provided in (21), is a smooth approximation of the non-continuous step function $H(\theta,\theta_{th})$.

Proof: See Appendix A. ∎

In the following table, we compute the limits of D_N and S_N using (10) and (11). Since $\sum_{n=1}^{N}\theta_n = N$, which is large, we set $\theta_{\text{th}} = 1$. In addition, when computing the limits, we have to consider a fixed Δ, i.e., fixed adjacent ports distance, since otherwise the elements of $\boldsymbol{\Sigma}$ vary with Δ (see (19)). Here we set $\Delta = W/99$, i.e., the distance between any two adjacent ports is fixed as if there are 100 ports. Then, we compute the limits of $D_N(1)$ and $S_N(1)$ using (10) and (11).

TABLE I
LIMITS OF $D_N(1)$ AND $S_N(1)$ FOR DIFFERENT W

W	0.5	1	2	3	4
Limit of $D_N(1)$	0.013	0.023	0.043	0.063	0.083
Limit of $S_N(1)$	0.9997	0.9996	0.9993	0.9990	0.9988

Table I shows that the limit of $D_N(1)$ is very small, i.e., only a small part of eigenvalues are larger than 1, and that of $S_N(1)$ is quite close to 1. Considering that $\frac{1}{N}\sum_{n=1}^{N}\theta_n = 1$, the energy of $\boldsymbol{\Sigma}$ is thus focused on the largest few eigenvalues. Hence, with a large N, $\tilde{g}_{j,k}^{(n)}$ in (7) can approximate $g_{j,k}^{(n)}$ using a small L. We will further show this by simulations.

To facilitate our analysis, as in [21], we further introduce two independent Gaussian variables to $\tilde{g}_{j,k}^{(n)}$ and get

$$\hat{g}_{j,k}^{(n)} = \sigma_{j,k}\sum_{m=1}^{L}\sqrt{\theta_m}u_{n,m}\left(a_{j,k}^{(m)} + ib_{j,k}^{(m)}\right) + \sigma_{j,k}\sqrt{1-\sum_{m=1}^{L}\theta_m u_{n,m}^2}\left(c_{j,k}^{(n)} + id_{j,k}^{(n)}\right), \tag{12}$$

where $a_{j,k}^{(m)}$, $b_{j,k}^{(m)}$, $c_{j,k}^{(n)}$, and $d_{j,k}^{(n)}$ are i.i.d. Gaussian variables with zero-mean and variance $\frac{1}{2}$. In contrast to $\tilde{g}_{j,k}^{(n)}$, the model $\hat{g}_{j,k}^{(n)}$ has two advantages. First, its variance is exactly $\sigma_{j,k}^2$. Second, as we will show in the next subsection, it makes the outage probability analysis more doable.

B. Outage Probability

Based on (6) and (12), the outage probability of user k can be approximated as

$$p_{\text{out},k} \approx \Pr\left\{\frac{|\hat{g}_{k,k}^{(1)}|}{|\hat{g}_{\bar{k},k}^{(1)}|} < r_k, \ldots, \frac{|\hat{g}_{k,k}^{(N)}|}{|\hat{g}_{\bar{k},k}^{(N)}|} < r_k\right\}. \tag{13}$$

For convenience, we denote $\Phi_k^{(n)} = |\hat{g}_{k,k}^{(n)}|/|\hat{g}_{\bar{k},k}^{(n)}|$. The following theorem provides the cumulative distribution function (CDF) of $\max\left\{\Phi_k^{(1)},\ldots,\Phi_k^{(N)}\right\}$.

Theorem 2. *With the approximation $\hat{g}_{j,k}^{(n)}$ provided in (12), the CDF of $\max\left\{\Phi_k^{(1)},\ldots,\Phi_k^{(N)}\right\}$ is given by (14) (see bottom of this page), where $F_{\Phi_k^{(n)}|(\boldsymbol{a}_{k,k},\boldsymbol{a}_{\bar{k},k},\boldsymbol{b}_{k,k},\boldsymbol{b}_{\bar{k},k})}(r_k)$ is provided in (15). In (15), $Q_1(\cdot,\cdot)$ and $I_0(\cdot)$ are respectively the Marcum Q-function of order 1 and the modified Bessel function of the first kind, and $\alpha_{j,k}^{(n)}$ as well as $\beta_{j,k}^{(n)}$ are given in (25).*

Proof: See Appendix B. ∎

Using Theorem 2, we could obtain the following approximation of the FAMA system's outage probability as

$$p_{\text{out},k}(r_k) \approx F_{\max\left\{\Phi_k^{(1)},\ldots,\Phi_k^{(N)}\right\}}(r_k), \text{ for } k = 1, 2. \tag{16}$$

IV. SIMULATION RESULTS

In this section, simulation results are presented to evaluate the performance of the two-user FAMA system and also the accuracy of the proposed approximation. For convenience, we assume equal transmit power for both users, i.e., $p_1 = p_2$. Moreover, since $\sigma_{j,k}$ can be regarded as the large-scale fading of the link from the j-th BS antenna to user k, we assume $\sigma_{1,k} = \sigma_{2,k}$, i.e., the channels from different antennas at the BS to both users experience the same large-scale fading. It is obvious that $\sigma_{j,k}$ does not affect the value of (6). Hence, in the simulations, we simply set $\sigma_{1,k} = \sigma_{2,k} = 1$. Notice that though the channel model $g_{j,k}^{(n)}$ in (4) has been significantly

$$F_{\max\left\{\Phi_k^{(1)},\ldots,\Phi_k^{(N)}\right\}}(r_k) = \frac{1}{\pi^{2L}}\int_{-\infty}^{+\infty}\cdots\int_{-\infty}^{+\infty}\exp\left\{-\sum_{m=1}^{L}\left[\left(a_{k,k}^{(m)}\right)^2 + \left(a_{\bar{k},k}^{(m)}\right)^2 + \left(b_{k,k}^{(m)}\right)^2 + \left(b_{\bar{k},k}^{(m)}\right)^2\right]\right\} \times \prod_{n=1}^{N} F_{\Phi_k^{(n)}|(\boldsymbol{a}_{k,k},\boldsymbol{a}_{\bar{k},k},\boldsymbol{b}_{k,k},\boldsymbol{b}_{\bar{k},k})}(r_k)\, da_{k,k}^{(1)}\cdots da_{k,k}^{(L)} da_{\bar{k},k}^{(1)}\cdots da_{\bar{k},k}^{(L)} db_{k,k}^{(1)}\cdots db_{k,k}^{(L)} db_{\bar{k},k}^{(1)}\cdots db_{\bar{k},k}^{(L)} \tag{14}$$

$$F_{\Phi_k^{(n)}|(\boldsymbol{a}_{k,k},\boldsymbol{a}_{\bar{k},k},\boldsymbol{b}_{k,k},\boldsymbol{b}_{\bar{k},k})}(r_k) = 1 - \int_0^{+\infty} Q_1\left(\sqrt{\frac{\alpha_{k,k}^{(n)}}{\beta_{k,k}^{(n)}}}, \frac{r_k z}{\sqrt{\beta_{k,k}^{(n)}}}\right)\frac{z}{\beta_{\bar{k},k}^{(n)}}\exp\left(-\frac{z^2+\alpha_{\bar{k},k}^{(n)}}{2\beta_{\bar{k},k}^{(n)}}\right) I_0\left(\frac{\sqrt{\alpha_{\bar{k},k}^{(n)}}}{\beta_{\bar{k},k}^{(n)}}z\right) dz \tag{15}$$

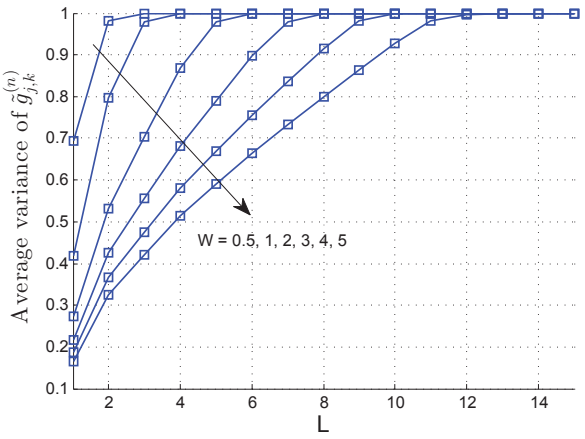

Fig. 1. Average variance of $\tilde{g}_{j,k}^{(n)}$ versus the approximation level L with $N = 100$.

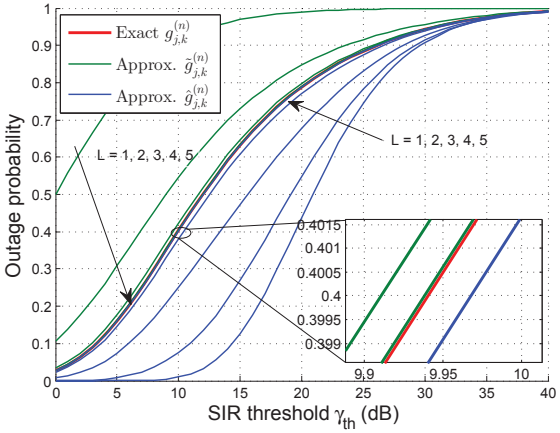

Fig. 2. Outage probability obtained based on $g_{j,k}^{(n)}$, $\tilde{g}_{j,k}^{(n)}$, and $\hat{g}_{j,k}^{(n)}$ versus the SIR threshold γ_{th} with $W = 1$ and $N = 100$.

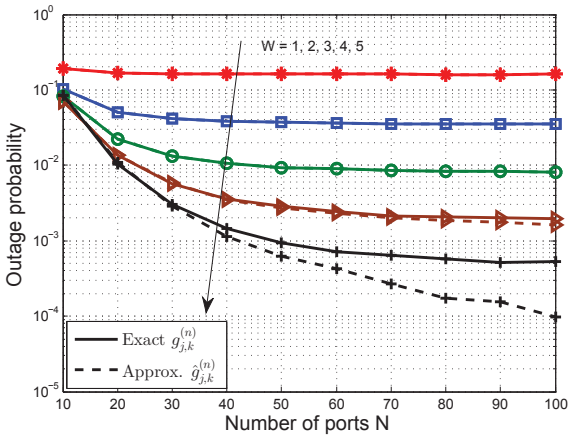

Fig. 3. Outage probability versus the number of ports N with $\gamma_{\text{th}} = 5dB$ and $L = 10$.

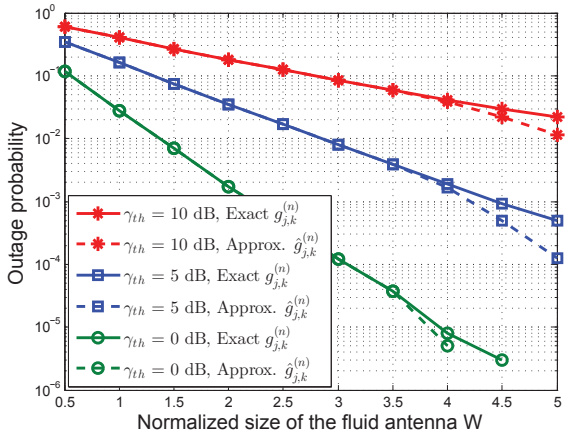

Fig. 4. Outage probability versus the normalized size of the fluid antenna W with $N = 100$ and $L = 10$.

simplified by $\hat{g}_{j,k}^{(n)}$, the CDF expression in Theorem 2 is hard to compute as it is a $4L$-fold integral (let alone the integral (15)). Here, we obtain the outage probability based on the channel models $g_{j,k}^{(n)}$, $\tilde{g}_{j,k}^{(n)}$, and $\hat{g}_{j,k}^{(n)}$ using Monte Carlo simulations. All the results were obtained by averaging over 10^6 independent channel realizations.

In Fig. 1, we show (in contrast to Table I) that the channel model $g_{j,k}^{(n)}$ can be approximated by taking into account only a few eigenvalues of $\boldsymbol{\Sigma}$. It is understood from (7) that $\tilde{g}_{j,k}^{(n)}$ follows Gaussian distribution with zero-mean and variance $\sum_{m=1}^{L} \theta_m u_{n,m}^2$ (since $\sigma_{j,k} = 1$). Fig. 1 shows the value of

$$\frac{1}{N} \sum_{n=1}^{N} \sum_{m=1}^{L} \theta_m u_{n,m}^2, \tag{17}$$

which can be seen as the average variance of $\tilde{g}_{j,k}^{(n)}, \forall n \in \{1, \cdots, N\}$. Since $\sum_{m=1}^{N} \theta_m u_{n,m}^2 = 1$, as L increases, the value of (17) should approach 1. Fig. 1 shows that this is true and can be realized by a small L. For example, when $W = 0.5$ and $W = 2$, the value of (17) is close to 1 with L, respectively, being 3 and 6. Therefore, we can approximate $g_{j,k}^{(n)}$ using either $\tilde{g}_{j,k}^{(n)}$ or $\hat{g}_{j,k}^{(n)}$ such that further analysis can be simplified.

In Fig. 2, we plot the outage probability of a user obtained by, respectively, using the exact channel model $g_{j,k}^{(n)}$, and its approximations $\tilde{g}_{j,k}^{(n)}$ and $\hat{g}_{j,k}^{(n)}$. It is illustrated that the outage probability resulted from $\tilde{g}_{j,k}^{(n)}$ and $\hat{g}_{j,k}^{(n)}$ is respectively an upper and lower bound to that based on $g_{j,k}^{(n)}$. As L increases, the bounds approach quickly to the curve obtained from $g_{j,k}^{(n)}$, and the approximation is good enough when $L = 4$ (with $W = 1$ and $N = 100$), which is consistent to the observation in Fig. 1. Since both $\tilde{g}_{j,k}^{(n)}$ and $\hat{g}_{j,k}^{(n)}$ can approximate $g_{j,k}^{(n)}$ well, and it is more convenient to analyze the outage probability based on $\hat{g}_{j,k}^{(n)}$, we depict only $g_{j,k}^{(n)}$ and $\hat{g}_{j,k}^{(n)}$ in subsequent results.

Figs. 3 and 4 investigate the impact of N and W on the outage probability. Note that for all the settings, we employ the same approximation level $L = 10$. Several observations can be made from these two figures. First of all, for small W, e.g., $W = 1$, the outage probability remains almost constant even when N increases. For larger W, the outage probability decreases first with N, indicating a great diversity gain and

then saturates. This is because the antenna ports are strongly correlated. With a fixed W, increasing N helps reduce the outage probability at the beginning, but can no longer bring diversity gains when N gets large since a smaller port distance causes strong inter-correlation. Secondly, it can be seen from Fig. 4 that for a given N, the system's outage probability can be dramatically reduced by increasing W. Moreover, Fig. 3 and Fig. 4 also show that with a small W, the solid and dashed lines completely coincide, but for a large W, e.g., $W = 4.5$ or $W = 5$, the outage probability obtained using $\hat{g}_{j,k}^{(n)}$ is obviously smaller than that resulted from $g_{j,k}^{(n)}$. This is because we set $L = 10$ for all the configurations. It is known from Fig. 1 that this is good enough for the approximation when W is smaller than 4. However, when $W = 5$, L has to be at least 12 such that the value of (17) approaches 1. In this case, the outage probability obtained from $\hat{g}_{j,k}^{(n)}$ is a lower bound to that based on $g_{j,k}^{(n)}$, which is also demonstrated by Fig. 1.

V. Conclusions

This paper investigated the outage performance of a two-user FAMA system under a fully correlated channel model that accurately accounts for the correlation between any two ports of the fluid antenna. We showed that each channel coefficient could be well approximated by L largest eigenvalues and $L \ll N$. With the approximation, the outage probability has been expressed as a $4L$-fold integral. Simulation results have verified the accuracy of the approximation and demonstrated great outage performance of the FAMA scheme.

Acknowledgments

This work was supported in part by the European Union's Horizon 2020 Research and Innovation Programme under Marie SkŁodowska-Curie Grant No. 101024636 and in part by the Engineering and Physical Sciences Research Council (EPSRC) under grant EP/W026813/1.

Appendix A
Proof of Theorem 1

It is known from (2) that $\boldsymbol{\Sigma}$ is a Hermitian Toeplitz matrix and can thus be re-expressed as

$$\boldsymbol{\Sigma} = \begin{bmatrix} \phi_0 & \phi_1 & \cdots & \phi_{N-1} \\ \phi_1 & \phi_0 & \ddots & \vdots \\ \vdots & \ddots & \ddots & \phi_1 \\ \phi_{N-1} & \cdots & \phi_1 & \phi_0 \end{bmatrix}. \tag{18}$$

According to (2) and [21, (47)], the coefficient ϕ_n can be expressed as the following Fourier form

$$\begin{aligned} \phi_n = J_0(2\pi n\Delta) &= \frac{1}{2\pi}\int_{-\pi}^{\pi} e^{i2\pi n\Delta \sin x} dx \\ &= \frac{1}{2\pi}\int_{-\pi}^{\pi} f(x)e^{-inx}dx, \text{ for } n = 0, \ldots, N-1, \end{aligned} \tag{19}$$

where

$$f(x) = \sum_{m=-\infty}^{m=+\infty} J_0(2\pi m\Delta)e^{imx}, \ \forall x \in [-\pi, \pi], \tag{20}$$

is a real and integrable function.

Then we apply [23, Theorem 1.1] to evaluate the limiting distribution of $D_N(\theta_{\text{th}})$ and $S_N(\theta_{\text{th}})$. Note that [23, Theorem 1.1] requires $H(\theta, \theta_{\text{th}})$ to be a continuous function. Thus, we replace $H(\theta, \theta_{\text{th}})$ by a smooth and analytic approximation. There are different ways to approximate a step function. Here we adopt the logistic function

$$\hat{H}(\theta, \theta_{\text{th}}) = \frac{1}{1 + e^{-2t(\theta - \theta_{\text{th}})}}, \tag{21}$$

as an approximation of $H(\theta, \theta_{\text{th}})$, where a larger t corresponds to a sharper transition at $\theta = \theta_{\text{th}}$. Then we have

$$\begin{aligned} \lim_{N\to+\infty} D_N(\theta_{\text{th}}) &= \lim_{N\to+\infty} \frac{1}{N}\sum_{n=1}^{N} H(\theta_n, \theta_{\text{th}}) \\ &\approx \lim_{N\to+\infty} \frac{1}{N}\sum_{n=1}^{N} \hat{H}(\theta_n, \theta_{\text{th}}) = \frac{1}{2\pi}\int_{-\pi}^{\pi} \hat{H}(f(x), \theta_{\text{th}})dx, \end{aligned} \tag{22}$$

where the last step follows by using [23, Theorem 1.1]. Hence, (10) is true. Analogously, based on the definition of $S_N(\theta_{\text{th}})$ in (9) and (21), (11) can be proven by following similar steps.

Appendix B
Proof of Theorem 2

For convenience, we denote $\boldsymbol{a}_{j,k} = (a_{j,k}^{(1)}, \ldots, a_{j,k}^{(L)})^T$ and $\boldsymbol{b}_{j,k} = (b_{j,k}^{(1)}, \ldots, b_{j,k}^{(L)})^T$. It is known from (12) that $\hat{g}_{j,k}^{(n)}$ is a Gaussian variable, and for a given $(\boldsymbol{a}_{j,k}, \boldsymbol{b}_{j,k})$, it follows

$$\begin{aligned} \hat{g}_{j,k}^{(n)}|(\boldsymbol{a}_{j,k}, \boldsymbol{b}_{j,k}) \sim \mathcal{CN}\Bigg(&\sigma_{j,k}\sum_{m=1}^{L}\sqrt{\theta_m}u_{n,m}\left(a_{j,k}^{(m)} + ib_{j,k}^{(m)}\right), \\ &\sigma_{j,k}^2\left(1 - \sum_{m=1}^{L}\theta_m u_{n,m}^2\right)\Bigg). \end{aligned} \tag{23}$$

Hence, $|\hat{g}_{j,k}^{(n)}||(\boldsymbol{a}_{j,k}, \boldsymbol{b}_{j,k})$ follows Rice or Rician distribution as shown below

$$|\hat{g}_{j,k}^{(n)}||(\boldsymbol{a}_{j,k}, \boldsymbol{b}_{j,k}) \sim \text{Rice}\left(\sqrt{\alpha_{j,k}^{(n)}}, \sqrt{\beta_{j,k}^{(n)}}\right), \tag{24}$$

where

$$\begin{aligned} \alpha_{j,k}^{(n)} &= \sigma_{j,k}^2\left[\left(\sum_{m=1}^{L}\sqrt{\theta_m}u_{n,m}a_{j,k}^{(m)}\right)^2 + \left(\sum_{m=1}^{L}\sqrt{\theta_m}u_{n,m}b_{j,k}^{(m)}\right)^2\right], \\ \beta_{j,k}^{(n)} &= \frac{\sigma_{j,k}^2}{2}\left(1 - \sum_{m=1}^{L}\theta_m u_{n,m}^2\right). \end{aligned} \tag{25}$$

Based on (24), we have

$$\begin{aligned} |\hat{g}_{k,k}^{(n)}||(\boldsymbol{a}_{k,k}, \boldsymbol{b}_{k,k}) &\sim \text{Rice}\left(\sqrt{\alpha_{k,k}^{(n)}}, \sqrt{\beta_{k,k}^{(n)}}\right), \\ |\hat{g}_{\bar{k},k}^{(n)}||(\boldsymbol{a}_{\bar{k},k}, \boldsymbol{b}_{\bar{k},k}) &\sim \text{Rice}\left(\sqrt{\alpha_{\bar{k},k}^{(n)}}, \sqrt{\beta_{\bar{k},k}^{(n)}}\right). \end{aligned} \tag{26}$$

Note that $|\hat{g}_{k,k}^{(n)}|$ and $|\hat{g}_{\bar{k},k}^{(n)}|$ are independent. Then for user k, $\Phi_k^{(n)}|(\boldsymbol{a}_{k,k}, \boldsymbol{a}_{\bar{k},k}, \boldsymbol{b}_{k,k}, \boldsymbol{b}_{\bar{k},k})$ is the ratio of two independent Rice random variables.

We now derive its CDF. For convenience, we consider two independent Rician variables $\hat{Z} \sim \text{Rice}(\sqrt{\alpha_1}, \sqrt{\beta_1})$, $Z \sim \text{Rice}(\sqrt{\alpha_2}, \sqrt{\beta_2})$, and denote $R = \hat{Z}/Z$. Then the CDF of R can be derived as

$$\begin{aligned} F_R(r) &= \Pr\{\hat{Z} \le rZ\} = \int_0^{+\infty} F_{\hat{Z}}(rz) f_Z(z) dz \\ &= 1 - \int_0^{+\infty} Q_1\left(\sqrt{\frac{\alpha_1}{\beta_1}}, \frac{rz}{\sqrt{\beta_1}}\right) \times \\ &\quad \frac{z}{\beta_2} \exp\left(-\frac{z^2+\alpha_2}{2\beta_2}\right) I_0\left(\frac{\sqrt{\alpha_2}}{\beta_2} z\right) dz, \end{aligned} \tag{27}$$

where the last step follows from directly using the CDF and probability density function (PDF) of Rice distribution, $Q_1(\cdot,\cdot)$ is the Marcum Q-function of order 1, and $I_0(\cdot)$ is the modified Bessel function of the first kind. Using (27), the CDF $F_{\Phi_k^{(n)}|(\boldsymbol{a}_{k,k}, \boldsymbol{a}_{\bar{k},k}, \boldsymbol{b}_{k,k}, \boldsymbol{b}_{\bar{k},k})}(r_k^{(n)})$ can be obtained directly and is provided in (15). For a given $(\boldsymbol{a}_{k,k}, \boldsymbol{a}_{\bar{k},k}, \boldsymbol{b}_{k,k}, \boldsymbol{b}_{\bar{k},k})$, (12) indicates that $\Phi_k^{(n)}, \forall n \in \{1, \cdots, N\}$ are independent of each other. Hence,

$$\begin{aligned} &F_{(\Phi_k^{(1)}, \cdots, \Phi_k^{(N)})|(\boldsymbol{a}_{k,k}, \boldsymbol{a}_{\bar{k},k}, \boldsymbol{b}_{k,k}, \boldsymbol{b}_{\bar{k},k})}(r_k^{(1)}, \cdots, r_k^{(N)}) \\ &\qquad = \prod_{n=1}^{N} F_{\Phi_k^{(n)}|(\boldsymbol{a}_{k,k}, \boldsymbol{a}_{\bar{k},k}, \boldsymbol{b}_{k,k}, \boldsymbol{b}_{\bar{k},k})}(r_k^{(n)}). \end{aligned} \tag{28}$$

The joint CDF of $(\Phi_k^{(1)}, \ldots, \Phi_k^{(N)})$ is thus the expectation of (28) over $(\boldsymbol{a}_{k,k}, \boldsymbol{a}_{\bar{k},k}, \boldsymbol{b}_{k,k}, \boldsymbol{b}_{\bar{k},k})$ and is provided in (29) at the bottom of this page. Since

$$F_{\max\left\{\Phi_k^{(1)}, \ldots, \Phi_k^{(N)}\right\}}(r_k) = F_{(\Phi_k^{(1)}, \ldots, \Phi_k^{(N)})}(r_k, \ldots, r_k), \tag{30}$$

by replacing all $r_k^{(n)}$ in (29) with r_k, we get (14).

REFERENCES

[1] E. G. Larsson, O. Edfors, F. Tufvesson, and T. L. Marzetta, "Massive MIMO for next generation wireless systems," *IEEE Commun. Mag.*, vol. 52, no. 2, pp. 186–195, Feb. 2014.

[2] N. Ye, J. An, and J. Yu, "Deep-learning-enhanced NOMA transceiver design for massive MTC: Challenges, state of the art, and future directions," *IEEE Wireless Commun.*, vol. 28, no. 4, pp. 66–73, Aug. 2021.

[3] F. Tariq, M. R. Khandaker, K. K. Wong, M. A. Imran, M. Bennis, and M. Debbah, "A speculative study on 6G," *IEEE Wireless Commun.*, vol. 27, no. 4, pp. 118–125, Aug. 2020.

[4] K. K. Wong, K. F. Tong, Y. Shen, Y. Chen, and Y. Zhang, "Bruce Lee-inspired fluid antenna system: Six research topics and the potentials for 6G," *Frontiers Commun. & Netw., section Wireless Commun.*, 3:853416, Mar. 2022.

[5] A. Shojaeifard *et al.*, "MIMO evolution beyond 5G through reconfigurable intelligent surfaces and fluid antenna systems," in *Proc. IEEE*, vol. 110, no. 9, pp. 1244–1265, Sept. 2022.

[6] S. J. Kar, A. Chakrabarty, and B. Sarkar, "Fluid antennas," in *IEEE Middle East Conf. Antennas and Propag. (MECAP)*, pp. 1–6, 20-22 Oct. 2010, Cairo, Egypt.

[7] G. J. Hayes, J.-H. So, A. Qusba, M. D. Dickey, and G. Lazzi, "Flexible liquid metal alloy (EGaIn) microstrip patch antenna," *IEEE Trans. Antennas Propag.*, vol. 60, no. 5, pp. 2151–2156, May 2012.

[8] A. Dey, R. Guldiken, and G. Mumcu, "Microfluidically reconfigured wideband frequency-tunable liquid-metal monopole antenna," *IEEE Trans. Antennas Propag.*, vol. 64, no. 6, pp. 2572–2576, Jun. 2016.

[9] A. Singh, I. Goode, and C. E. Saavedra, "A multistate frequency reconfigurable monopole antenna using fluidic channels," *IEEE Antennas Wireless Propag. Lett.*, vol. 18, no. 5, pp. 856–860, May 2019.

[10] D. Rodrigo, B. A. Cetiner and L. Jofre, "Frequency, radiation pattern and polarization reconfigurable antenna using a parasitic pixel layer," *IEEE Trans. Antennas Propag.*, vol. 62, no. 6, pp. 3422–3427, Jun. 2014.

[11] K. K. Wong, A. Shojaeifard, K. F. Tong, and Y. Zhang, "Fluid antenna systems," *IEEE Trans. Wireless Commun.*, vol. 20, no. 3, pp. 1950–1962, Mar. 2021.

[12] K. K. Wong, A. Shojaeifard, K. F. Tong, and Y. Zhang, "Performance limits of fluid antenna systems," *IEEE Commun. Lett.*, vol. 24, no. 11, pp. 2469–2472, Nov. 2020.

[13] Z. Chai, K. K. Wong, K. F. Tong, Y. Chen, and Y. Zhang, "Port selection for fluid antenna systems," *IEEE Commun. Lett.*, vol. 26, no. 5, pp. 1180–1184, Feb. 2022.

[14] L. Tlebaldiyeva, G. Nauryzbayev, S. Arzykulov, A. Eltawil and T. Tsiftsis, "Enhancing QoS through fluid antenna systems over correlated Nakagami-m fading channels," in *Proc. IEEE Wireless Commun. Netw. Conf. (WCNC)*, pp. 78–83, 10-13 Apr. 2022, Austin, TX, USA.

[15] C. Psomas, G. M. Kraidy, K. K. Wong, and I. Krikidis, "On the diversity and coded modulation design of fluid antenna systems," [Online] arXiv preprint arXiv:2205.01962, 2022.

[16] P. Mukherjee, C. Psomas, and I. Krikidis, "On the level crossing rate of fluid antenna systems," [Online] arXiv preprint arXiv:2205.01711, 2022.

[17] K. K. Wong and K. F. Tong, "Fluid antenna multiple access," *IEEE Trans. Wireless Commun.*, vol. 21, no. 7, pp. 1950–1962, Jul. 2022.

[18] K. K. Wong, K. F. Tong, Y. Chen and Y. Zhang, "Closed-form expressions for spatial correlation parameters for performance analysis of fluid antenna systems," *IET Electronics Lett.*, vol. 58, no. 11, pp. 454–457, Apr. 2022.

[19] K. K. Wong, K. F. Tong, Y. Chen, and Y. Zhang, "Extra-large MIMO enabling slow fluid antenna massive access for millimeter-wave bands," accepted in *IET Electronics Lett.*.

[20] N. C. Beaulieu and K. T. Hemachandra, "Novel simple representations for Gaussian class multivariate distributions with generalized correlation," *IEEE Trans. Inform. Theory*, vol. 57, no. 12, pp. 8072–8083, Dec. 2011.

[21] M. Khammassi, A. Kammoun, and M.-S. Alouini, "A new analytical approximation of the fluid antenna system channel," [Online] arXiv preprint arXiv:2203.09318, 2022.

[22] W. C. Jakes Jr., *Microwave mobile communications*, Wiley, New York, 1974.

[23] S. Serra, "On the extreme eigenvalues of Hermitian (block) Toeplitz matrices," *Linear Alg. Appl.*, vol. 270, no. 1-3, pp. 109–129, 1998.

$$\begin{aligned} F_{(\Phi_k^{(1)}, \ldots, \Phi_k^{(N)})}(r_k^{(1)}, \ldots, r_k^{(N)}) &= \mathbb{E}_{(\boldsymbol{a}_{k,k}, \boldsymbol{a}_{\bar{k},k}, \boldsymbol{b}_{k,k}, \boldsymbol{b}_{\bar{k},k})}\left[\prod_{n=1}^{N} F_{\Phi_k^{(n)}|(\boldsymbol{a}_{k,k}, \boldsymbol{a}_{\bar{k},k}, \boldsymbol{b}_{k,k}, \boldsymbol{b}_{\bar{k},k})}(r_k^{(n)})\right] \\ &= \frac{1}{\pi^{2L}} \int_{-\infty}^{+\infty} \cdots \int_{-\infty}^{+\infty} \exp\left\{-\sum_{m=1}^{L}\left[\left(a_{k,k}^{(m)}\right)^2 + \left(a_{\bar{k},k}^{(m)}\right)^2 + \left(b_{k,k}^{(m)}\right)^2 + \left(b_{\bar{k},k}^{(m)}\right)^2\right]\right\} \\ &\quad \times \prod_{n=1}^{N} F_{\Phi_k^{(n)}|(\boldsymbol{a}_{k,k}, \boldsymbol{a}_{\bar{k},k}, \boldsymbol{b}_{k,k}, \boldsymbol{b}_{\bar{k},k})}(r_k^{(n)}) \, da_{k,k}^{(1)} \cdots da_{k,k}^{(L)} da_{\bar{k},k}^{(1)} \cdots da_{\bar{k},k}^{(L)} db_{k,k}^{(1)} \cdots db_{k,k}^{(L)} db_{\bar{k},k}^{(1)} \cdots db_{\bar{k},k}^{(L)} \end{aligned} \tag{29}$$